ACS APPLIED BIO MATERIALS

www.acsabm.org Article

$Co_2V_2O_7$ Particles with Intrinsic Multienzyme Mimetic Activities as an Effective Bioplatform for Ultrasensitive Fluorometric and Colorimetric Biosensing

Xiaotong Zhang, Gaojie Han, Ruiqi Zhang, Ze Huang, Hao Shen, Ping Su, Jiayi Song,* and Yi Yang*

Cite This: *ACS Appl. Bio Mater.* 2020, 3, 1469−1480 Read Online

ACCESS | Metrics & More | Article Recommendations | Supporting Information

ABSTRACT: Nanozymes with various activities have attracted much attention owing to their great potential in the fields of biochemical analysis and environmental monitoring. Herein, for the first time, granular $Co_2V_2O_7$ particles were synthesized using a simple hydrothermal method with pH regulation, and the triple-enzyme (oxidase-like, peroxidase-like, and catalase-like) activities and catalytic mechanisms of the prepared particles were systematically studied. On the basis of the excellent oxidase-like and peroxidase-like activities of $Co_2V_2O_7$ particles, respectively, a colorimetric biosensor for detecting glutathione in health products (linear range: 2.5−20 μM) and a fluorescent platform for detecting glucose in human serum (linear range: 0.1−80 μM) were established, both of which had good selectivity and reliability. In particular, the fluorescence detection system exhibited ultrahigh sensitivity for H_2O_2, with a linear range of 0.008−3.2 μM, and a detection limit (0.002 μM) far superior to most reported in the literature to date. Furthermore, a one-step strategy for glucose detection was established to replace the traditional complicated two-step detection method, resulting in a more convenient detection process. These findings indicate the significant application prospects of $Co_2V_2O_7$ particles in the field of biocatalysis and provide useful information for the future development of cobalt vanadate nanomaterials as enzyme mimics.

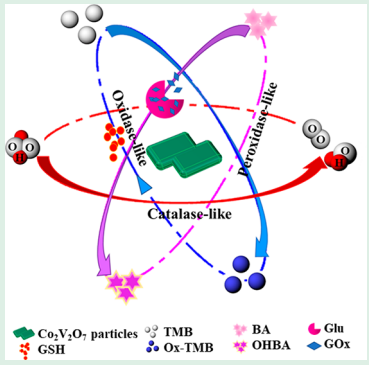

KEYWORDS: *nanozymes, $Co_2V_2O_7$ particles, triple-enzyme mimetics, biosensing, one-step, glutathione/hydrogen peroxide/glucose detection*

INTRODUCTION

Nanozymes, which are nanomaterials that show enzyme catalytic activity, have been widely used in various fields, such as immune analysis,[1,2] disease diagnosis,[3−5] environmental protection,[6,7] and disinfectant and antibacterial applications.[8] Numerous studies have shown that nanomaterials can mimic various natural enzymes, such as oxidase,[9] peroxidase,[10,11] catalase,[12] and superoxide dismutase.[13] Therefore, nanozymes have become ideal substitutes for natural enzymes. To date, most research has focused on the activity of single enzymes.[14,15] However, nanomaterials with multienzyme activities and high catalytic performance tend to have greater advantages and application prospects. Unfortunately, only a few nanomaterials, such as Co_3O_4 nanoplates,[1,16,17] Mn_3O_4[18] and CuO[19] nanoparticles, have exhibited high multienzyme activities and achieved satisfactory applications. The development of novel nanozyme materials with multienzyme activities to improve catalytic efficiency and simplify catalytic steps remains challenging.

Glucose is the main energy-generating substance in organisms, and it has always been a hot topic of research in the field of nanozymes.[20−23] Recently, some nanomaterials with multienzyme activities have been developed for glucose detection. For example, V_6O_{13} nanotextiles[24] exhibit good specificity for glucose, with a fluorescent system established for glucose sensing. Furthermore, $NiFe_2O_4$ magnetic nanoparticles[25] have been successfully applied to achieve glucose detection in urine samples. Although these nanozymes with multienzyme activities show improved performance, some common problems limit their practical application, such as low sensitivity and inconvenient testing. Peroxidase-like nanozyme of the multienzyme activities materials and natural glucose oxidase (GOx) are the most common combination used for glucose detection in these examples. However, the optimal catalytic pH of peroxidase-like nanozymes tends to cause natural GOx to denature. Therefore, the widely reported glucose detection method based on nanozymes with multienzyme activity still requires a two-step method.[26−28] Specifically, assay completion requires two incubations in different buffers, inevitably leading to drawbacks, such as unstable intermediate products, increased processing time, a laborious secondary pH adjustment, and material waste, which are major obstacles to the detection process. To overcome these limitations, new types of nanozymes with multienzyme

Received: December 2, 2019
Accepted: February 6, 2020
Published: February 6, 2020

https://dx.doi.org/10.1021/acsabm.9b01107
ACS Appl. Bio Mater. 2020, 3, 1469−1480

activities need be developed urgently to improve the cascade reaction efficiency and exchange the two-step procedure for a one-step glucose detection.

Binary metal oxides are able to synergistically enhance electron/ion conductivity, reversibility, and mechanical stability. Among them, cobalt vanadium oxides ($Co_xV_2O_{5+x}$, where x is 1,[29,30] 2,[31,32] or 3[33,34]) have attracted much attention owing to their complex crystal structures and magnetic properties. To date, the applications of cobalt vanadate have mainly focused on its electrochemical field, such as electrocatalytic oxygen release reaction,[35] asymmetric supercapacitor electrodes,[36] and lithium ion batteries.[37] Co-based nanomaterials, such as Co_3O_4,[16] $CoFe_2O_4$,[38] and $NiCo_2O_4$[39] nanoparticles, and V-based nanomaterials, such as V_2O_5,[40] V_6O_{13},[24] and VO_x,[41,42] have been reported to possess superior nanozyme-like catalytic activity owing to their mixed valence and structural advantages. Among these nanozymes, the mixed valence state of the metal oxide is always considered an important reason for its multienzyme activities.[18] Interestingly, cobalt vanadate has not only the high specific capacity and mixed valence of Co but also the stability of the VO_x amorphous array. Inspired by these studies, we hypothesized that cobalt vanadate could exert the synergistic catalytic effect of bimetals and possess excellent multienzyme activities. However, the multienzyme properties of cobalt vanadate have yet to be reported.

In this study, cubic granular $Co_2V_2O_7$ particles were synthesized using a simple hydrothermal method with pH regulation, and the triple-enzyme activities were studied in detail (Scheme 1). On the basis of the excellent oxidase-like and peroxidase-like activities of $Co_2V_2O_7$ particles, two biosensors were designed to realize the visual detection of glutathione (GSH) and ultrasensitive fluorescence detection of H_2O_2 and glucose, respectively. Notably, as the optimal catalytic pH for the peroxidase-like activity of the material coincided with that of GOx, one-step detection of glucose was achieved, making the reaction more efficient and precise. To our knowledge, the enzymatic activity of $Co_2V_2O_7$ particles is reported for the first time. This research demonstrates the great application prospects of $Co_2V_2O_7$ particles in biochemical analysis.

Scheme 1. Schematic Illustration of Multienzyme Mimetic Activities of $Co_2V_2O_7$ Particles

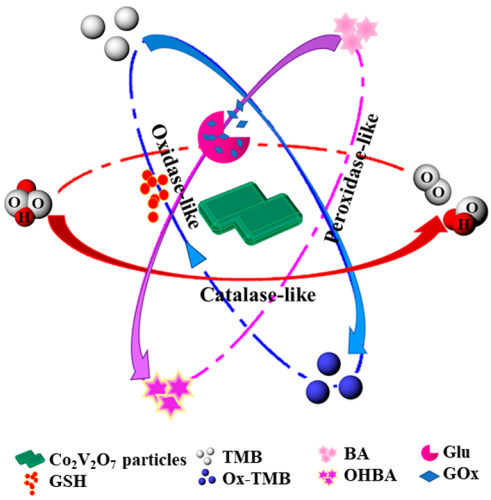

EXPERIMENTAL SECTION

Preparation of $Co_2V_2O_7$ Particles. $Co_2V_2O_7$ particles were synthesized using a simple hydrothermal method inspired by the report of Yu et al.[43] In detail, NH_4VO_3 (1.0 mmol) was dissolved in deionized water (30 mL) and stirred at 75 °C to obtain a transparent solution. Next, deionized water (30 mL) containing 1.0 mmol $Co(NO_3)_2{\cdot}6H_2O$ was added dropwise to the above solution to form a final suspension. The solution pH was then adjusted to 7 by adding 2.0 M NaOH dropwise, and the resulting suspension was transferred to a sealed autoclave, which was heated at 180 °C for 15 h. Finally, the brown-green product was collected by centrifugation, washed several times with deionized water and anhydrous ethanol, and then dried in a vacuum oven at 60 °C for 24 h. As a control, other cobalt vanadate samples were obtained by adjusting the solution pH to 3 and 11.

Kinetic Analysis. The entire reaction system was conducted in a 5 mL reaction solution (50 mM HAc-NaAC, pH 3.0, 35 °C) with 30 μg mL^{-1} $Co_2V_2O_7$ particles. The steady-state kinetic analysis of the peroxidase-like activity was performed by varying the 3,3′,5,5′-tetramethylbenzidine (TMB) concentration and fixing the H_2O_2 concentration, or vice versa. The Michaelis−Menten constant was calculated using the Lineweaver−Burk plot, as follows:

$$1/V = K_m/V_m(1/[S] + 1/K_m) \quad (1)$$

where V is the initial velocity, V_m stands for the maximum reaction velocity, [S] represents the substrate concentration, and K_m corresponds to the Michaelis−Menten constant.

Investigation of Oxidase-like Activity of $Co_2V_2O_7$ Particles. $Co_2V_2O_7$ particles with oxidase-like activity can directly oxidize substrates in the presence of oxygen. TMB, 2,2′-azino-bis(3-ethylbenzothiazoline-6-sulfonic acid) (ABTS), and *o*-phenylenediamine (OPD) were selected as substrates, and an ultraviolet spectrophotometer was used to detect the absorbance of the reaction system at 652, 420, and 450 nm, respectively. The specific operation was performed as follows: 30 μg mL^{-1} $Co_2V_2O_7$ particles and 0.3 mM TMB, 0.6 mM ABTS or 0.6 mM OPD were added to HAc-NaAc buffer solution (pH 2.5, 50 mM), with the total volume of the reaction system kept at 5 mL, and the mixed solution was incubated at 30 °C for 20 min. Furthermore, to verify the importance of O_2 in the reaction system, the absorbance curves of two reaction systems using TMB as substrate under air and nitrogen flow conditions were compared, respectively.

Investigation of Peroxidase-like Activity of $Co_2V_2O_7$ Particles. $Co_2V_2O_7$ particles with peroxidase-like activity can catalyze the oxidation of benzoic acid (BA) to produce fluorescent products in the presence of H_2O_2. In detail, $Co_2V_2O_7$ particles (150 μL, 1 mg mL^{-1}), BA (500 μL, 14 mM), and H_2O_2 (100 μL, 8 mM) were added to phosphate buffered saline (PBS) solution (4.25 mL, pH 5.0, 50 mM). The reaction was conducted at 30 °C for 20 min, and the fluorescence intensity of the system was detected (excitation at 298 nm, emission at 405 nm).

Investigation of Catalase-like Activity of $Co_2V_2O_7$ Particles. $Co_2V_2O_7$ particles with catalase-like activity can decompose H_2O_2 to produce oxygen, which can be detected by a dissolved oxygen meter. $Co_2V_2O_7$ solution (5 mL) with different concentrations and H_2O_2 (5 mL, 600 mM) were added to PBS buffer solution (20 mL, pH 5.0, 50 mM). The

https://dx.doi.org/10.1021/acsabm.9b01107
ACS Appl. Bio Mater. 2020, 3, 1469−1480

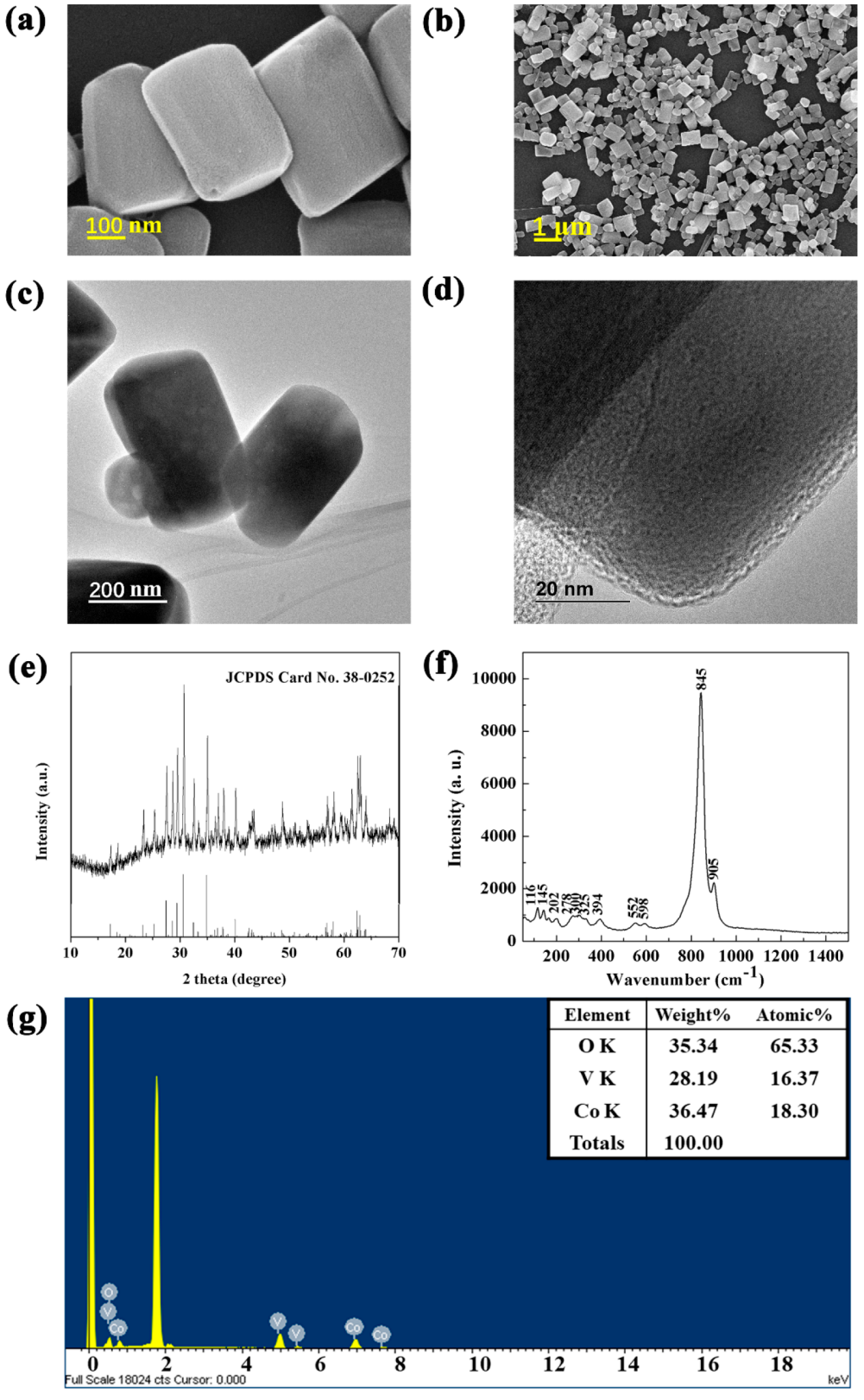

Figure 1. (a, b) SEM images, (c, d) TEM images, (e) XRD pattern, (f) Raman spectrum (excitation at 633 nm), and (g) EDX spectrum of $Co_2V_2O_7$ particles.

oxygen content in the system was measured every 10 s for 15 min.

Colorimetric Detection of GSH Using $Co_2V_2O_7$ Particles Oxidase Mimic. Colorimetric detection of GSH was performed as follows: $Co_2V_2O_7$ particles (150 μL, 1 mg mL^{-1}), TMB (300 μL, 5 mM), and varying volumes of GSH (1.0 mM) were added to HAc-NaAc buffer (pH 2.5, 50 mM), with the total volume of the reaction system kept at 5 mL. The

https://dx.doi.org/10.1021/acsabm.9b01107
ACS Appl. Bio Mater. 2020, 3, 1469−1480

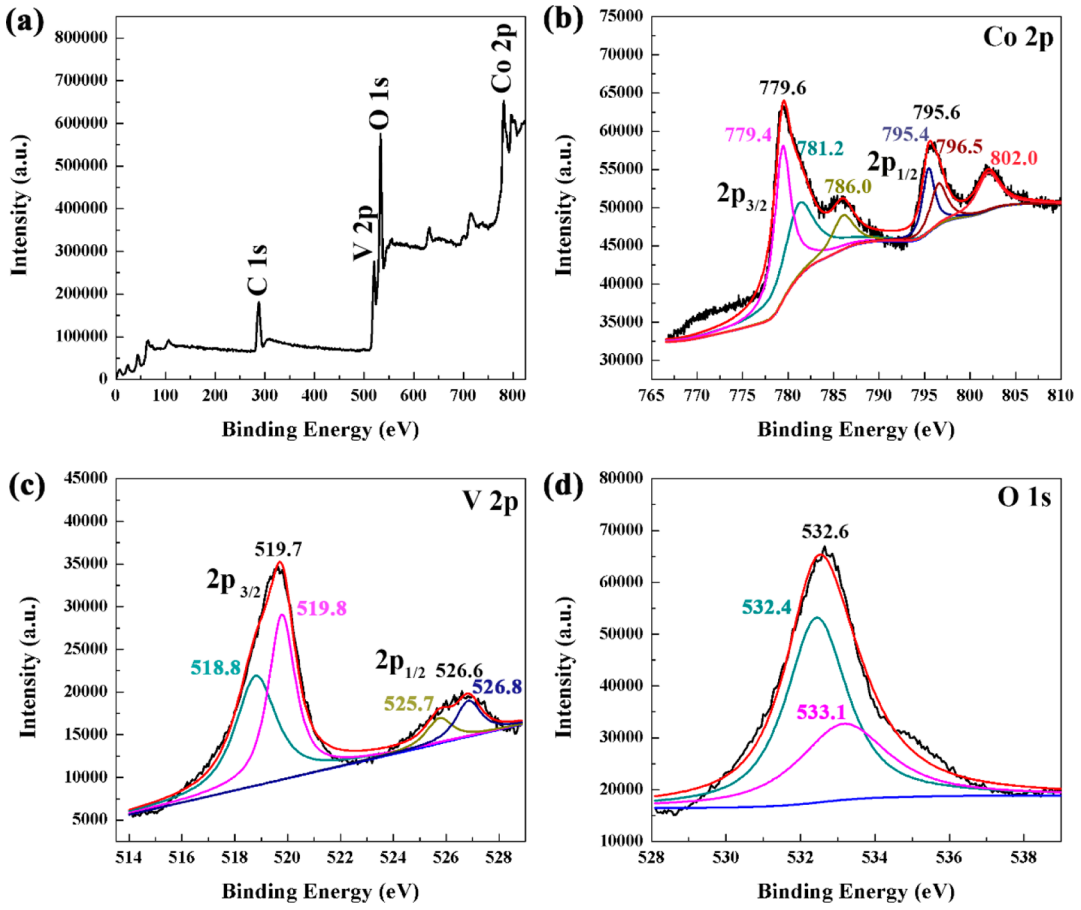

Figure 2. XPS spectra of $Co_2V_2O_7$ particles: (a) Survey spectrum, (b) Co 2p, (c) V 2p, and (d) O 1s.

reaction lasted 24 min at 35 °C, and the absorbance at 652 nm was measured using an UV−vis spectrophotometer.

One-Step Fluorescent Detection of Glucose Using $Co_2V_2O_7$ Particles Peroxidase Mimic. $Co_2V_2O_7$ particles (350 μL, 1 mg mL^{-1}), BA solution (500 μL, 14 mM), and different volumes of glucose solution (20 μM), and GOx (100 μL, 0.1 mg mL^{-1}) were added sequentially to PBS solution (pH 5.0, 50 mM). The 5 mL final system was incubated at 30 °C for 15 min. The reaction system without glucose was used as a blank sample, $\Delta F = F$ (glucose, 405 nm) − F (blank, 405 nm). Similarly, the above glucose solution was replaced with human serum, which was diluted 100 times to ensure that the concentration was within the linear detection range of the method. A 500 μL of serum sample was added to the reaction system each time, and the other detection steps were the same as above. To further demonstrate the specificity of this method, the fluorescence intensity of the system was detected by replacing glucose with fructose, maltose, sucrose, and galactose.

RESULTS AND DISCUSSION

Characterization of $Co_2V_2O_7$ Particles. The size and morphology of $Co_2V_2O_7$ particles were investigated by scanning electron microscopy (SEM). As shown in Figure 1a,b, the prepared $Co_2V_2O_7$ particles mostly possessed a cubic granular shape with an identical aspect ratios of nearly 1.5:1, with widths of about 250 nm. Transmission electron microscopy (TEM; Figure 1c,d) further indicated the cubic granular morphology of the prepared materials, in agreement with the SEM images. Crystallographic information on the $Co_2V_2O_7$ particles was obtained by X-ray diffraction (XRD), with the diffraction peaks (Figure 1e) in good agreement with the characteristic peaks of $Co_2V_2O_7$ (JCPDS card no. 38-0252) in the standard spectrum. Raman spectroscopy was also used to characterize the prepared materials, as shown in Figure 1f. The bands at 905 and 845 cm^{-1} were attributed to symmetric and asymmetric stretching of the VO_4 units, respectively.[30] Furthermore, the peaks located at 278 and 394 cm^{-1} and 300, 552, and 598 cm^{-1} were assigned to V−O and V−O−V stretching modes, respectively, indicating the successful preparation of $Co_2V_2O_7$. The EDX spectrum of the prepared nanomaterial (Figure 1g) showed that it was comprised 36.47 Co, 28.19% V, and 35.34% O by weight, with a V/O/Co atomic ratio of about 1:1:3.5, which matched well with the molecular formula $Co_2V_2O_7$.

To obtain further surface chemical information for the $Co_2V_2O_7$ particles, XPS spectrum was measured (Figure 2). The Co 2p, V 2p, O 1s, and C 1s regions were readily observed in the survey spectrum (Figure 2a). The Co 2p spectrum (Figure 2b) is typically classified into $2p_{3/2}$ and $2p_{1/2}$. The deconvoluted $2p_{3/2}$ peak consisted of +2 and +3 oxidation states at 779.4 and 781.2 eV, respectively.[44] The 6.4 eV energy gap between the satellite peak (786.0 eV) and the Co $2p_{3/2}$ main peak (779.6 eV) provided evidence for the presence of Co(II).[45] Similarly, the peaks at 519.7 and 526.6 eV were assigned to V $2p_{3/2}$ and V $2p_{1/2}$, respectively (Figure 2c). The peak at 519.7 eV decomposed to 518.8 and 519.8 eV, which demonstrated the presence of +4 and +5 oxidation states.[44,46]

https://dx.doi.org/10.1021/acsabm.9b01107
ACS Appl. Bio Mater. 2020, 3, 1469−1480

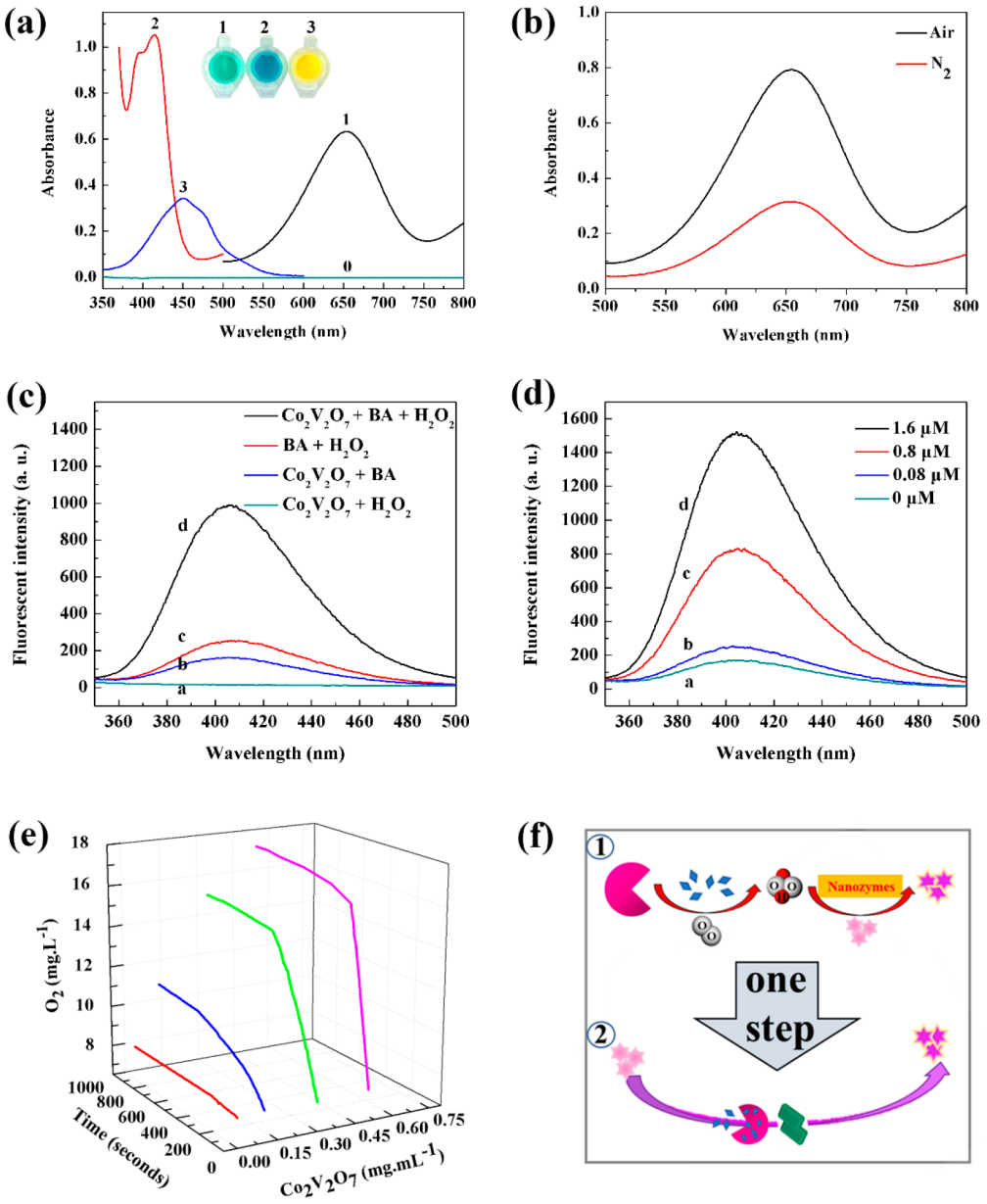

Figure 3. (a) Absorption spectra of different chromogenic substrates and corresponding digital photographs under catalytic oxidation of $Co_2V_2O_7$ particles: (0) Blank, (1) TMB, (2) ABTS, and (3) OPD. (b) Effect of dissolved oxygen on $Co_2V_2O_7$-TMB system. (c) Fluorescence spectra of the system under different conditions. (d) Effect of different H_2O_2 concentrations on $Co_2V_2O_7$-BA system. (e) Effect of different concentration of $Co_2V_2O_7$ on O_2 generation from H_2O_2 decomposition. (f) Glucose detection schematic: (1) traditional two-step method; (2) one-step method using $Co_2V_2O_7$.

These above results confirmed the presence of Co^{2+}, Co^{3+}, V^{4+}, and V^{5+} on the surface of the $Co_2V_2O_7$ particles. The different environmental states of oxygen in the $Co_2V_2O_7$ particles are shown in Figure 2d. The two peaks with binding energies of 532.4 and 533.1 eV can be combined to characterize the broad O 1s peak. The former is a characteristic oxygen peak of metal oxide, while the latter indicates the presence of hydroxyl groups or adsorbed water on the $Co_2V_2O_7$ particles surface.[45]

The pH value during the preparation process was a critical factor affecting the particle morphology, which further contributed to the distinct enzymatic activities. The effects of pH on the morphology and enzymatic activity of the prepared materials were investigated, and whether the morphology and crystal structure of the materials could be regulated and controlled by changing the pH was investigated. The XRD patterns of the cobalt vanadate nanomaterials obtained at pH 3 and 11 were compared. As shown in Figure S1a, the diffraction peaks of materials (pH 3 and pH 11) were both relatively weak, indicating poor crystallinity and that these products might have amorphous forms. Investigation of enzymatic activity is shown in Figure S1b. The material with a pH of 11 exhibited the lowest oxidase-like activity. Although a slightly higher activity was observed by the material with pH of 3 compared with that of the material with a pH of 7, the stability is not very good during the detection process. Interestingly, the SEM images (Figure S2) indicated that material (a) (pH 3) comprised rod-like structures of different lengths, which were closely interlaced and had an average width of about 80 nm. Meanwhile, material (c) (pH 11) showed a large amount of irregular aggregation with an amorphous state. These results

https://dx.doi.org/10.1021/acsabm.9b01107
ACS Appl. Bio Mater. 2020, 3, 1469−1480

indicated that pH regulation played a key role in the synthesis of materials in this study. Furthermore, the morphology and structure of cobalt vanadate were easily adjusted by pH regulation, resulting in different sizes and a transition between crystalline and amorphous forms. In comparison, the $Co_2V_2O_7$ nanomaterials prepared at pH 7 showed higher crystallinity and better stability, so it was selected for the follow-up investigation of enzyme activity.

Oxidase-like Catalytic Activity of $Co_2V_2O_7$ Particles. To investigate the oxidase-like activity of the prepared $Co_2V_2O_7$ particles, three commonly used substrates, TMB, ABTS, and OPD, were applied. The reaction system without substrate was used as a blank experiment. As shown in Figure 3a, TMB, ABTS, and OPD were catalyzed by $Co_2V_2O_7$ particles without H_2O_2 to form the corresponding chromogenic products. The blank group without substrate did not have any UV absorption peaks. These results indicated that $Co_2V_2O_7$ particles possessed broad-spectrum oxidase-like activity and were not specific to the above three oxidase substrates.

According to the literature,[24] TMB oxidation is caused by the action of dissolved oxygen. Therefore, we conducted a verification experiment in which N_2 was passed through the reaction system for 30 min to remove oxygen. Subsequently, the $Co_2V_2O_7$ particles dispersions and TMB solution were transferred to the N_2-filled bottle using a syringe. The reaction system without nitrogen treatment was applied under the same conditions for comparison. Figure 3b showed that the 652 nm absorbance of the N_2-filled reaction system was significantly lower than that of the case which was untreated. In this process, dissolved oxygen participates in electron transfer as an electron acceptor, which is the actual oxidant.[47] Under acidic conditions, the TMB adsorbed on the surface of $Co_2V_2O_7$ particles provided a large number of electrons to the system, thereby increasing the electron density and surface mobility of $Co_2V_2O_7$ particles. Meanwhile, electrons were rapidly transferred to oxygen adsorbed on the surface of the $Co_2V_2O_7$ particles, combining with TMB to form an electron-transfer complex. In other words, $Co_2V_2O_7$ particles enhance catalytic efficiency by accelerating electron transfer throughout the catalytic reaction. In order to verify the oxidase-like catalytic mechanism, we investigated the electrocatalytic behavior of TMB oxidation by $Co_2V_2O_7$ particles modified glassy carbon electrode (GCE) using cyclic voltammetry (CV). As shown in Figure S3, there was no current change in the system with only acetate buffer solution. One pair of TMB redox peaks could be observed under a bare GCE. The GCE modified with $Co_2V_2O_7$ particles significantly increased the current value. It was proved that $Co_2V_2O_7$ particles had the ability to accelerate electron transfer.

To investigate the effect of leaching ions on the catalytic activity, we incubated $Co_2V_2O_7$ particles in acetate buffer solution (pH 2.5) for 2 h and then centrifuged to obtain the supernatant to catalyze TMB. The results (Figure S4) showed that the catalytic activity was not related to the leaching ions, and the oxidase-like activity of $Co_2V_2O_7$ particles originated from the nanomaterial itself.

To achieve the optimal catalytic effect, several important parameters were examined, as shown in Figure S5 for details. Since the oxidase-like activity of $Co_2V_2O_7$ particles was carried out at a relatively low pH value (pH 2.5), the stability of $Co_2V_2O_7$ was investigated (Figure S6). With the prolonged soaking time of the $Co_2V_2O_7$ in the buffer solution (pH 2.5), the catalytic activity showed a downward trend. However, even if the time was as long as 80 min, the relative activity could still reach more than 80%, so it is feasible to investigate the oxidase-like activity in the reaction system at this pH value.

Peroxidase-like Catalytic Activity of $Co_2V_2O_7$ Particles. The peroxidase-like activity was explored by introducing H_2O_2 and fluorescent indicator BA into the system. H_2O_2 can be catalyzed by the peroxidase-like nanozyme to form a hydroxyl radical ($^{\bullet}OH$), which can react with BA to form hydroxybenzoic acid (BAOH). When excited at 298 nm, the corresponding characteristic emission peaks of BAOH were generated at 405 nm.[27] As shown in Figure 3c, when substrate BA was not added to the system, no characteristic fluorescence peak was observed. In the presence of BA, introducing $Co_2V_2O_7$ particles or H_2O_2 can cause the system to produce a weak fluorescence response. This is due to $Co_2V_2O_7$ particles possessing oxidase-like activity, which can catalyze BA oxidation directly in the presence of O_2, while H_2O_2 can produce trace $^{\bullet}OH$ under weak acidic conditions and then combine with BA to obtain fluorescence products. These phenomena were consistent with literature reports.[24,28] When $Co_2V_2O_7$ particles, BA, and H_2O_2 were present in the system, the fluorescence characteristic peak of the system at 405 nm was strong. These results also implied that the generation of $^{\bullet}OH$ was closely related to the peroxidase-like catalytic mechanism of $Co_2V_2O_7$ particles, similar to other nanozymes.[27,28] As shown in Figure 3d, the fluorescence intensity of the system at 405 nm increased with increasing H_2O_2 concentration, indicating that the $^{\bullet}OH$ content was increasing, which further proved that $Co_2V_2O_7$ particles catalyzed H_2O_2 to produce $^{\bullet}OH$. Furthermore, even if the H_2O_2 concentration was as low as 0.08 μM, the system could still detect obvious fluorescence intensity, which reflected the ultrasensitivity of the $Co_2V_2O_7$-BA-H_2O_2 detection system.

In order to further explore whether other reactive oxygen species (ROS) have affected the peroxidase-like catalytic mechanism, we used electron paramagnetic resonance (EPR) technology to detect ROS in the reaction system. As a spin capture reagent, 5,5-dimethyl-1-pyrroline n-oxide (DMPO) can react with oxygen-centered free radicals to form more stable free radicals adducts.[48] We used deionized water and dimethyl sulfoxide (DMSO) as solvents to prepare 30 mM DMPO to capture the hydroxyl and superoxide radicals in the system, respectively. It can be seen in Figure S7a(ii) that the system incorporating $Co_2V_2O_7$ particles had a significant characteristic spectrum of DMPO/$^{\bullet}OH$ adduct with the intensity of 1:2:2:1,[1,18] indicating that $^{\bullet}OH$ did exist in the system. The small mixed peaks may be caused by insufficient purity of DMPO, or they may be derived from other ROS. In order to verify this, we also tested the superoxide radicals in the system. It can be seen in Figure S7b(ii) that the addition of $Co_2V_2O_7$ particles only produced some weak peaks. Overall, the catalytic mechanism of peroxidase-like enzymes is mainly derived from $^{\bullet}OH$ in the system.

Several important parameters (temperature, pH, etc.) were investigated to achieve optimized catalytic activity for the prepared nanozyme (for detailed discussion, see Figure S8). Interestingly, unlike most other peroxide mimetic enzymes, the optimal catalytic activity of $Co_2V_2O_7$ particles was achieved at pH 5.0, which was consistent with the optimal pH of natural GOx, providing the possibility of subsequent one-step glucose detection.

https://dx.doi.org/10.1021/acsabm.9b01107
ACS Appl. Bio Mater. 2020, 3, 1469−1480

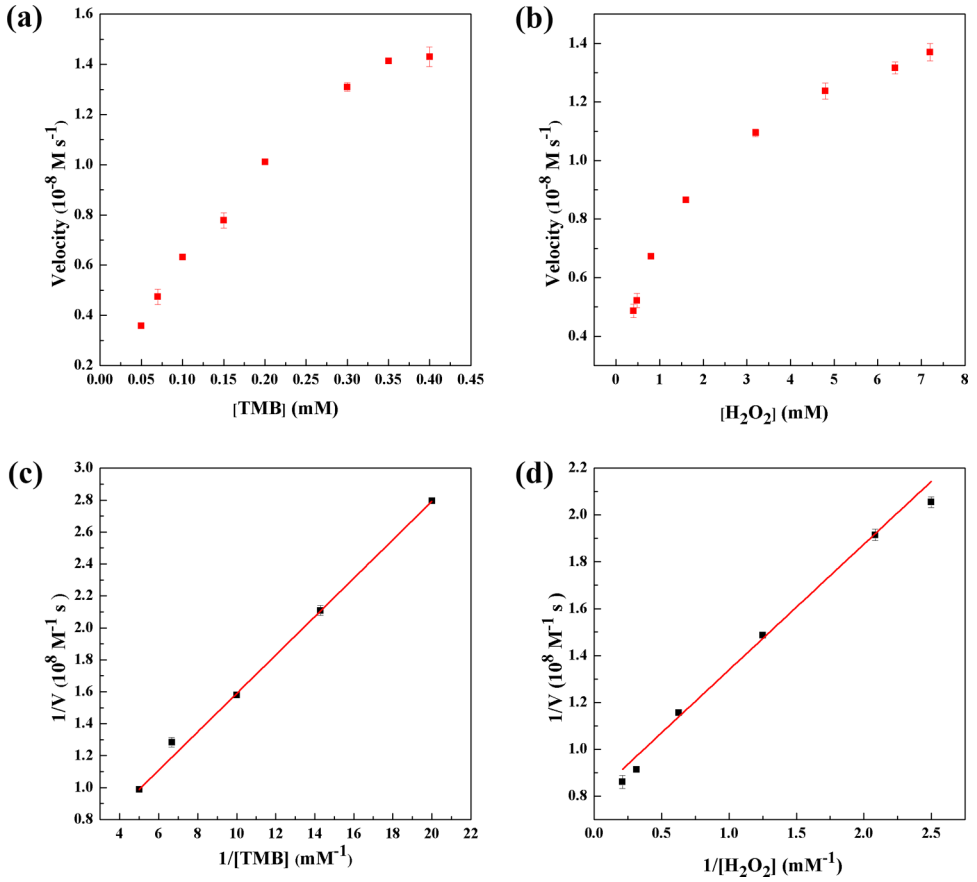

Figure 4. Steady-state kinetic analysis for $Co_2V_2O_7$ particles. Michaelis−Menten plots for (a) TMB substrate and (b) H_2O_2 substrate. Double reciprocal plots for (c) TMB substrate and (d) H_2O_2 substrate. The fixed concentration for H_2O_2 and TMB was 1.6 mM and 0.3 mM, respectively.

Catalase-like Catalytic Activity of $Co_2V_2O_7$ Particles. Considering the excellent oxidase-like and peroxidase-like activities of the prepared $Co_2V_2O_7$ particles, we next investigated whether the prepared materials possessed catalase-like activity by investigating the effects of different concentrations of $Co_2V_2O_7$ particles on H_2O_2 decomposition. We recorded the oxygen content in the reaction solution every 10 s for 15 min using a portable dissolved oxygen meter. Four different $Co_2V_2O_7$ particles concentrations (0, 0.1, 0.3, and 0.5 mg mL^{-1}) were selected for comparison. As shown in Figure 3e, the dissolved oxygen concentration increased with increasing $Co_2V_2O_7$ particles concentration, indicating that $Co_2V_2O_7$ particles could directly catalyze H_2O_2 decomposition to produce O_2. According to a previous study,[1] Co^{3+}/Co^{2+} has a high standard oxidation−reduction potential, and H_2O_2 is more readily oxidized by Co^{3+} to form water and oxygen. This supported the theory that $Co_2V_2O_7$ particles possess intrinsic catalase-like activity.

Measurement of Steady-State Kinetic Parameters of $Co_2V_2O_7$ Particles. The steady-state kinetic parameters of the reaction system were investigated using TMB and H_2O_2 as substrates within a certain concentration range. The Michaelis−Menten curves of TMB and H_2O_2 are shown in Figure 4a,b. Based on these, double reciprocal Lineweaver−Burk curves were plotted (Figure 4c,d), and main kinetic parameters including K_m and V_{max} were calculated. The K_m values of $Co_2V_2O_7$ particles toward TMB and H_2O_2 were 0.311 mM and 0.669 mM, respectively, which were both clearly lower than that of horseradish peroxidase (HRP) (Table S1), suggesting that $Co_2V_2O_7$ particles exhibited a higher affinity toward the substrates than to the natural enzyme. This might be due to the existence of more "active sites" on the surface of the $Co_2V_2O_7$ particles compared to HRP.[2,49] Interestingly, compared with other binary transition-metal oxides (Table S1), $Co_2V_2O_7$ particles had certain advantages in both their affinity for TMB and H_2O_2. It was speculated that $Co_2V_2O_7$ particles not only possessed the strong attraction ligand ability of the cobalt ion but also the stability of the VO_x amorphous array, such that the synergistic effect between bimetals can be exerted to a greater extent, ensuring a suitable gap for combination with substrates.[50]

GSH Detection Using the $Co_2V_2O_7$ Particles-Based Colorimetric Biosensor. GSH regulates oxidative stress and reduces oxidative damage, and nanozymes with oxidase-like activity can be used to detect such antioxidants.[51] Therefore, we investigated whether the prepared $Co_2V_2O_7$ particles could be applied to the detection of GSH. Figure 5a showed that with the increase of GSH concentration, the color of reaction system gradually faded, which was consistent with the decreasing absorbance of the reaction system at 652 nm. Under the optimized reaction conditions, a calibration curve for detecting GSH was obtained. Figure 5b showed the calibration data of ΔA_{652} ($\Delta A_{652} = A(\text{blank}) - A(\text{GSH})$) to GSH concentration. A (blank) represents the absorbance value at 652 nm without GSH. The ΔA_{652} value was proportional to GSH concentration from 2.5−20 μM with a detection limit of 0.64 μM ($S/N = 3$). To test the selectivity of this approach, we examined the colorimetric response of this assay system under

https://dx.doi.org/10.1021/acsabm.9b01107
ACS Appl. Bio Mater. 2020, 3, 1469−1480

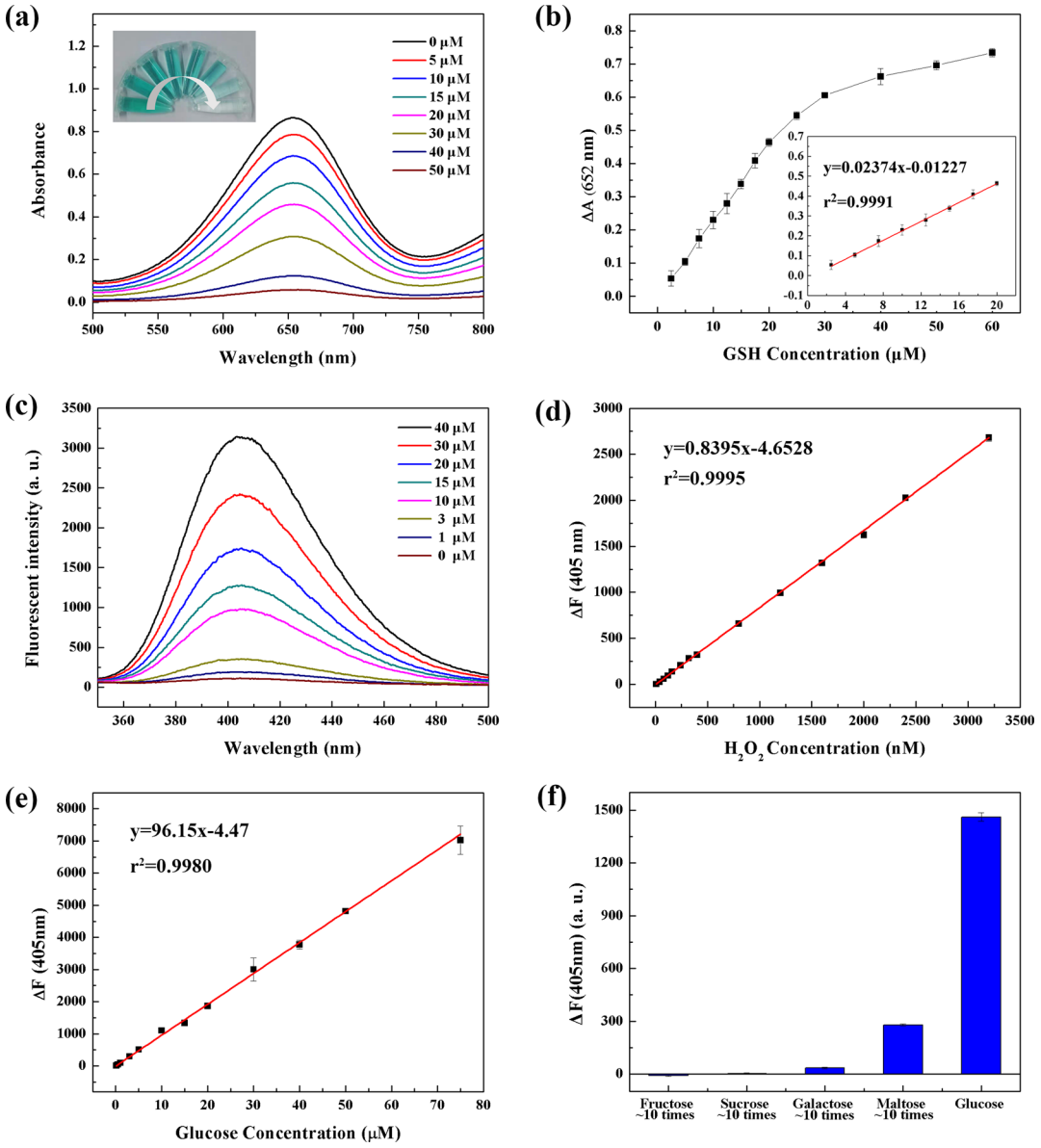

Figure 5. (a) The change of UV−vis absorbance of $Co_2V_2O_7$-TMB system with the concentration of GSH. (b) Calibration curve of GSH concentration. (c) The change of fluorescence intensity of $Co_2V_2O_7$-BA system with the concentration of glucose. (d) Linear calibration curve of H_2O_2 concentration determination. (e) Linear calibration curve of glucose determination. (f) Selective determination of glucose detection in the $Co_2V_2O_7$-BA system.

latent interferences (eight common amino acids, five carbohydrates, and five cations) that might exist together with GSH in health supplements. As shown in Figure S9, even if the concentration of the potential disturber was 100 times higher than that of GSH, it did not significantly affect GSH detection. Subsequently, the established biosensor was applied to determine GSH in capsules. From Table S2, it could be observed that the standard recovery rate and standard deviation were both within a reasonable range, which indicated the feasibility of this method for GSH detection in practical applications.

H_2O_2 and Glucose Detection Using the $Co_2V_2O_7$ Particles-Based Ultrasensitive Fluorometric Platform. On the basis of the peroxidase-like activity of $Co_2V_2O_7$ particles, a $Co_2V_2O_7$-BA fluorescence platform was established for supersensitive H_2O_2 determination and one-step glucose determination. As shown in Figure 5c, the concentration of glucose was positively correlated with the fluorescence intensity of the system (excitation at 298 nm, emission at 405 nm), where $\Delta F_{405} = F$ (glucose) − F (blank). A standard curve for H_2O_2/glucose detection was plotted under the optimal reaction conditions. As shown in Figure 5d, the H_2O_2 detection system exhibited a superior linear relationship with H_2O_2 over a wide concentration range of 8−3200 nM. The linear regression equation was as follows: $\Delta F = 0.8395C_{H_2O_2}$ (nM) − 4.6528 (r^2 = 0.9995). The detection limit was as low as 2 nM, which was much lower than most reported in the literature to date[17,24,28,43,52−55] (Table 1). This indicated that our method has ultrahigh sensitivity and great potential for the detection of trace H_2O_2. This might be due to some properties of the $Co_2V_2O_7$ nanomaterials, such as unique structure, uniform size, and synergistic catalysis between different metal ions.[45] Strikingly, Co^{3+}/Co^{2+} with higher oxygen reduction potential and vanadium ions with mixed valence state

https://dx.doi.org/10.1021/acsabm.9b01107
ACS Appl. Bio Mater. 2020, 3, 1469−1480

Table 1. Linear Range and Detection Limit of H_2O_2 Detected by Different Nanozymes

catalyst	method	linear range (μM)	LOD (μM)	ref
$FeVO_4$	colorimetric	2−40	0.2	43
Co_3O_4	colorimetric	50−25000	10	17
$CoFe_2O_4$	colorimetric	20−6000	20	54
α-$AgVO_3$	colorimetric	60−200	2	53
CA-BiPtNC@GO	colorimetric	0.01−1500	0.01	52
$Cu_{0.5}/Co_{0.5}$-MOG	fluorometric	1.0−10	0.081	55
Fe_3O_4 MMs	fluorometric	0.04−8.0	0.008	28
V_6O_{13} NTs	fluorometric	8.0−1600.0	6.41	24
$Co_2V_2O_7$	Fluorometric	0.008−3.2	0.002	This work

contribute greatly to the interpretation of the excellent catalytic performance of the corresponding materials, which were demonstrated by the previous reports.[1,41] Furthermore, the $Co_2V_2O_7$-BA detection system maintained excellent peroxidase activity under the optimized conditions (pH 5.0, Figure S8a). This was different to most other literature studies, which reported an optimal pH of about 3.0 or 4.0.[56−59] We suspected that the reason for the optimal peroxidase pH was the presence of mixed valence cobalt with ultrahigh electron mobility in the material.[45]

In recent years, the combination of GOx and nanozymes with peroxide activity has been the main strategy for detecting glucose, which is highly dependent on the activities of GOx and nanozymes. As the optimum pH (5.0) of GOx[60,61] is often inconsistent with that of nanozymes, the detection process is generally conducted in two steps (Figure 3f), namely, a first step of glucose oxidation by GOx and a second step of H_2O_2 decomposition by a nanozyme with peroxide activity through secondary pH regulation of the reaction solution to initiate a typical color reaction in the presence of a color-developing reagent. However, the optimal pH of the $Co_2V_2O_7$ particles peroxidase was 5.0 in the current study, which was consistent with the optimal pH of GOx. This superior nature indicates that the traditional two-step colorimetric glucose biosensing can be converted into a one-step (Figure 3f), making the operation more simple and faster. To verify this conjecture, we tried to add $Co_2V_2O_7$ particles, GOx, glucose, and BA directly into the buffer (pH 5) for the reaction, with the results shown in Figure 5e. For the glucose detection system, the linear range was 0.1−80 μM, and the linear regression equation was as follows: $\Delta F = 96.15C$ (μM) − 4.47 ($r^2 = 0.9980$), with a detection limit of 0.03 μM. This confirmed the feasibility of the one-step method in this system. The glucose detection system also possessed good selectivity, and when the concentration of other sugars was 10 times higher than that of glucose (Figure 5f), no significant interference with the reaction system was observed. The fluorometric platform was then applied to detect glucose in human blood samples, which were diluted 100-fold, as shown in the Table 2. The glucose detection value was close to the value provided by the hospital, indicating that the method has high accuracy in detecting glucose from blood samples.

CONCLUSIONS

In summary, $Co_2V_2O_7$ particles were synthesized through pH adjustment using a simple hydrothermal method. We have demonstrated for the first time that the nanomaterial possesses intrinsic triple-enzyme (oxidase-like, peroxidase-like, and catalase-like) activities and studied the catalytic mechanisms by cyclic voltammetry and EPR technology. $Co_2V_2O_7$ particles exhibit extraordinary enzymatic properties due to the synergistic effect between the mixed valence bimetallic ions. Based on this, a visual colorimetric biosensor and an ultrasensitive fluorescence platform are constructed. It is worth mentioning that the prepared materials exhibit ultrahigh sensitivity toward H_2O_2, and the detection limit is far superior to most literature reports. Moreover, the successful detection of GSH in health products and the one-step determination of glucose in human serum are sufficient to demonstrate the practical application value of the biosensor. This work not only shows the broad application prospects of $Co_2V_2O_7$ particles in biochemical analysis and clinical diagnosis other than electrochemical fields but also provides some ideas for the development of new inorganic nanozymes. Since the pH required by the bioplatform in the detection process is not close to neutral, this will become the direction we continue to explore in the future for in vivo detection.

ASSOCIATED CONTENT

Supporting Information

The Supporting Information is available free of charge at https://pubs.acs.org/doi/10.1021/acsabm.9b01107.

Chemicals and materials, XRD patterns, SEM images and enzyme-like activities of the cobalt vanadate materials prepared under different pH values, cyclic voltammograms, effect of leaching ions on catalysis, optimization, stability, DMPO spin−trapping EPR spectra, comparison of apparent kinetic parameters, selectivity assay of $Co_2V_2O_7$-TMB system, analytical results of GSH determination in real samples (PDF)

AUTHOR INFORMATION

Corresponding Authors

Jiayi Song − *Beijing Key Laboratory of Environmentally Harmful Chemical Analysis, College of Chemistry, Beijing University of Chemical Technology, Beijing 100029, P.R.*

Table 2. Determination of Glucose in Human Serum Samples (n = 3)

	glucose concentration (mmol L^{-1})					
sample[a]	hospital method	proposed method (±SD)	glucose added (mmol L^{-1})	glucose found (mmol L^{-1}) (±SD)	recovery (%)	RSD (%)
1	4.4	4.43 ± 0.28	5.00	9.67 ± 0.21	104.93	2.12
			10.00	14.60 ± 0.14	101.82	0.96
2	4.8	4.97 ± 0.07	5.00	10.04 ± 0.11	101.33	1.14
			10.00	14.99 ± 0.38	99.02	2.51

[a]The human serum samples were from the School Medical Clinic of Beijing University of Chemical Technology.

https://dx.doi.org/10.1021/acsabm.9b01107
ACS Appl. Bio Mater. 2020, 3, 1469−1480

China; orcid.org/0000-0002-8724-6884; Email: songjy@mail.buct.edu.cn

Yi Yang − *Beijing Key Laboratory of Environmentally Harmful Chemical Analysis, College of Chemistry, Beijing University of Chemical Technology, Beijing 100029, P.R. China;* orcid.org/0000-0002-4091-8532; Phone: +86-10-64441521; Email: yangyi@mail.buct.edu.cn

Authors

Xiaotong Zhang − *Beijing Key Laboratory of Environmentally Harmful Chemical Analysis, College of Chemistry, Beijing University of Chemical Technology, Beijing 100029, P.R. China*

Gaojie Han − *Beijing Key Laboratory of Environmentally Harmful Chemical Analysis, College of Chemistry, Beijing University of Chemical Technology, Beijing 100029, P.R. China*

Ruiqi Zhang − *Beijing Key Laboratory of Environmentally Harmful Chemical Analysis, College of Chemistry, Beijing University of Chemical Technology, Beijing 100029, P.R. China*

Ze Huang − *Beijing Key Laboratory of Environmentally Harmful Chemical Analysis, College of Chemistry, Beijing University of Chemical Technology, Beijing 100029, P.R. China*

Hao Shen − *Beijing Key Laboratory of Environmentally Harmful Chemical Analysis, College of Chemistry, Beijing University of Chemical Technology, Beijing 100029, P.R. China*

Ping Su − *Beijing Key Laboratory of Environmentally Harmful Chemical Analysis, College of Chemistry, Beijing University of Chemical Technology, Beijing 100029, P.R. China*

Complete contact information is available at: https://pubs.acs.org/10.1021/acsabm.9b01107

Notes

The authors declare no competing financial interest.

■ ACKNOWLEDGMENTS

This work was supported by the National Natural Science Foundation of China (grant no. 21675008).

■ REFERENCES

(1) Dong, J. L.; Song, L. N.; Yin, J. J.; He, W. W.; Wu, Y. H.; Gu, N.; Zhang, Y. Co_3O_4 Nanoparticles with Multi-enzyme Activities and Their Application in Immunohistochemical Assay. *ACS Appl. Mater. Interfaces* **2014**, *6*, 1959−1970.

(2) Gao, L. Z.; Zhuang, J.; Nie, L.; Zhang, J. B.; Zhang, Y.; Gu, N.; Wang, T. H.; Feng, J.; Yang, D. L.; Perrett, S.; Yan, X. Y. Intrinsic Peroxidase-like Activity of Ferromagnetic Nanoparticles. *Nat. Nanotechnol.* **2007**, *2*, 577−583.

(3) Wang, X. Y.; Qin, L.; Zhou, M.; Lou, Z. P.; Wei, H. Nanozyme Sensor Arrays for Detecting Versatile Analytes from Small Molecules to Proteins and Cells. *Anal. Chem.* **2018**, *90*, 11696−11702.

(4) Mu, X. Y.; Wang, J. Y.; Li, Y. H.; Xu, F. J.; Long, W.; Ouyang, L. F.; Liu, H. H.; Jing, Y. Q.; Wang, J. Y.; Dai, H. T.; Liu, Q.; Sun, Y. M.; Liu, C. L.; Zhang, X. D. Redox Trimetallic Nanozyme with Neutral Environment Preference for Brain Injury. *ACS Nano* **2019**, *13*, 1870−1884.

(5) Yin, M. Y.; Duan, Z. Q.; Zhang, C. X.; Feng, L. P.; Wan, Y. Q.; Cai, Y. Y.; Liu, H.; Li, S.; Wang, H. A Visualized Colorimetric Detection Strategy for Heparin in Serum Using a Metal-free Polymer Nanozyme. *Microchem. J.* **2019**, *145*, 864−871.

(6) Ma, C. M.; Ma, Y.; Sun, Y. F.; Lu, Y.; Tian, E. L.; Lan, J. F.; Li, J. L.; Ye, W. C.; Zhang, H. X. Colorimetric Determination of Hg^{2+} in Environmental Water Based on The Hg^{2+}-stimulated Peroxidase Mimetic Activity of MoS_2-Au Composites. *J. Colloid Interface Sci.* **2019**, *537*, 554−561.

(7) Shi, H. J.; Liu, Y.; Qu, R.; Li, Y. F.; Ma, R. J.; An, Y. L.; Shi, L. Q. A Facile One-pot Method to Prepare Peroxidase-like Nanogel Artificial Enzymes for Highly Efficient and Controllable Catalysis. *Colloids Surf., B* **2019**, *174*, 352−359.

(8) Xu, B. L.; Wang, H.; Wang, W. W.; Gao, L. Z.; Li, S. S.; Pan, X. T.; Wang, H. Y.; Yang, H. L.; Meng, X. Q.; Wu, Q. W.; Zheng, L. R.; Chen, S. M.; Shi, X. H.; Fan, K. L.; Yan, X. Y.; Liu, H. Y. A Single-Atom Nanozyme for Wound Disinfection Applications. *Angew. Chem., Int. Ed.* **2019**, *58*, 4911−4916.

(9) Molinari, M.; Symington, A. R.; Sayle, D. C.; Sakthivel, T. S.; Seal, S.; Parker, S. C. Computer-Aided Design of Nanoceria Structures as Enzyme Mimetic Agents: The Role of Bodily Electrolytes on Maximizing Their Activity. *ACS Applied Bio Materials* **2019**, *2*, 1098−1106.

(10) Lian, M. L.; Zhang, S.; Chen, J.; Liu, X. J.; Chen, X.; Yang, W. S. Self-Assembling Peptide Artificial Enzyme as an Efficient Detection Prober and Inhibitor for Cancer Cells. *ACS Applied Bio Materials* **2019**, *2*, 2185−2191.

(11) Wang, J.; Yang, X.; Wei, T.; Bao, J.; Zhu, Q.; Dai, Z. Fe-Porphyrin-Based Covalent Organic Framework As a Novel Peroxidase Mimic for a One-Pot Glucose Colorimetric Assay. *ACS Applied Bio Materials* **2018**, *1*, 382−388.

(12) Liu, Y.; Wu, H. H.; Li, M.; Yin, J. J.; Nie, Z. pH Dependent Catalytic Activities of Platinum Nanoparticles with Respect to the Decomposition of Hydrogen Peroxide and Scavenging of Superoxide and Singlet Oxygen. *Nanoscale* **2014**, *6*, 11904−11910.

(13) He, W. W.; Zhou, Y. T.; Wamer, W. G.; Hu, X.; Wu, X.; Zheng, Z.; Boudreau, M. D.; Yin, J. J. Intrinsic Catalytic Activity of Au Nanoparticles with Respect to Hydrogen Peroxide Decomposition and Superoxide Scavenging. *Biomaterials* **2013**, *34*, 765−73.

(14) Yan, L.; Ren, H.; Guo, Y. Y.; Wang, G.; Liu, C. Y.; Wang, Y. B.; Liu, X.; Zeng, L. X.; Liu, A. H. Rock Salt Type NiO Assembled on Ordered Mesoporous Carbon as Peroxidase Mimetic for Colorimetric Assay of Gallic Acid. *Talanta* **2019**, *201*, 406−412.

(15) Zhang, H. J.; Chen, J.; Yang, Y. L.; Wang, L.; Li, Z.; Qiu, H. D. Discriminative Detection of Glutathione in Cell Lysates Based on Oxidase-Like Activity of Magnetic Nanoporous Graphene. *Anal. Chem.* **2019**, *91*, 5004−5010.

(16) Wang, Q. Q.; Chen, J. X.; Zhang, H.; Wu, W. W.; Zhang, Z. Q.; Dong, S. J. Porous Co_3O_4 Nanoplates with pH-switchable Peroxidase- and Catalase-like Activity. *Nanoscale* **2018**, *10*, 19140−19146.

(17) Mu, J. S.; Wang, Y.; Zhao, M.; Zhang, L. Intrinsic Peroxidase-like Activity and Catalase-like Activity of Co_3O_4 Nanoparticles. *Chem. Commun.* **2012**, *48*, 2540−2542.

(18) Singh, N.; Savanur, M. A.; Srivastava, S.; D'Silva, P.; Mugesh, G. A Redox Modulatory Mn_3O_4 Nanozyme with Multi-Enzyme Activity Provides Efficient Cytoprotection to Human Cells in a Parkinson's Disease Model. *Angew. Chem., Int. Ed.* **2017**, *56*, 14267−14271.

(19) Hu, A. L.; Deng, H. H.; Zheng, X. Q.; Wu, Y. Y.; Lin, X. L.; Liu, A. L.; Xia, X. H.; Peng, H. P.; Chen, W.; Hong, G. L. Self-cascade Reaction Catalyzed by CuO Nanoparticle-based Dual-functional Enzyme Mimics. *Biosens. Bioelectron.* **2017**, *97*, 21−25.

(20) Wei, H.; Wang, E. Fe_3O_4 Magnetic Nanoparticles as Peroxidase Mimetics and Their Applications in H_2O_2 and Glucose Detection. *Anal. Chem.* **2008**, *80*, 2250−2254.

(21) Guo, Y. Y.; Yan, L.; Zhang, R. Y.; Ren, H.; Liu, A. H. CoO-supported Ordered Mesoporous Carbon Nanocomposite Based Nanozyme with Peroxidase-like Activity for Colorimetric Detection of Glucose. *Process Biochem.* **2019**, *81*, 92−98.

(22) Han, L.; Shi, J. G.; Liu, A. H. Novel Biotemplated MnO_2 1D Nanozyme with Controllable Peroxidase-like Activity and Unique Catalytic Mechanism and Its Application for Glucose Sensing. *Sens. Actuators, B* **2017**, *252*, 919−926.

(23) Han, L.; Zeng, L. X.; Wei, M. D.; Li, C. M.; Liu, A. H. A V_2O_3-ordered Mesoporous Carbon Composite with Novel Peroxidase-like Activity towards the Glucose Colorimetric Assay. *Nanoscale* **2015**, *7*, 11678−85.

(24) Li, H. F.; Wang, T.; Wang, Y. F.; Wang, S. M.; Su, P.; Yang, Y. Intrinsic Triple-Enzyme Mimetic Activity of V_6O_{13} Nanotextiles:

Mechanism Investigation and Colorimetric and Fluorescent Detections. *Ind. Eng. Chem. Res.* **2018**, *57*, 2416−2425.
(25) Su, L.; Qin, W. J.; Zhang, H.; Rahman, Z. U.; Ren, C. L.; Ma, S. D.; Chen, X. G. The Peroxidase/Catalase-like Activities of MFe_2O_4 (M = Mg, Ni, Cu) MNPs and Their Application in Colorimetric Biosensing of Glucose. *Biosens. Bioelectron.* **2015**, *63*, 384−391.
(26) Liu, Q. Y.; Yang, Y. T.; Li, H.; Zhu, R. R.; Shao, Q.; Yang, S. G.; Xu, J. J. NiO Nanoparticles Modified with 5,10,15,20-tetrakis(4-carboxyl pheyl)-porphyrin: Promising Peroxidase Mimetics for H_2O_2 and Glucose Detection. *Biosens. Bioelectron.* **2015**, *64*, 147−153.
(27) Luo, W.; Li, Y.-S.; Yuan, J.; Zhu, L.; Liu, Z.; Tang, H.; Liu, S. Ultrasensitive Fluorometric Determination of Hydrogen Peroxide and Glucose by Using Multiferroic $BiFeO_3$ Nanoparticles as a Catalyst. *Talanta* **2010**, *81*, 901−907.
(28) Shi, Y.; Su, P.; Wang, Y. Y.; Yang, Y. Fe_3O_4 Peroxidase Mimetics as a General Strategy for the Fluorescent Detection of H_2O_2-involved Systems. *Talanta* **2014**, *130*, 259−264.
(29) Mondal, C.; Sasmal, A. K.; Yusuf, S. M.; Mukadam, M. D.; Pal, J.; Ganguly, M.; Pal, T. Modified Hydrothermal Reaction (MHT) for $CoV_2O_6{\cdot}4H_2O$ Nanowire Formation and the Transformation to $CoV_2O_6{\cdot}2H_2O$ Single-crystals for Antiferromagnetic Ordering and Spin-flop. *RSC Adv.* **2014**, *4*, 56977−56983.
(30) Tang, Y.; Zhou, J.; Liu, J.; Liu, L. X.; Liang, S. Q. Facile Synthesis of Cobalt Vanadium Oxides and Their Applications in Lithium Batteries. *Int. J. Electrochem. Sci.* **2013**, *8*, 1138−1145.
(31) Almukhlifi, H. A.; Burns, R. C. Oxidative Dehydrogenation of Isobutane to Isobutene by Pyrovanadates, $M_2V_2O_7$, where M(II)= Mn, Co, Ni, Cu and Zn, and Co_2VO_4 and ZnV_2O_4: The Effect of Gold Nanoparticles. *J. Mol. Catal. A: Chem.* **2015**, *408*, 26−40.
(32) Luo, Y. Z.; Xu, X.; Zhang, Y. X.; Chen, C. Y.; Zhou, L.; Yan, M. Y.; Wei, Q. L.; Tian, X. C.; Mai, L. Q. Graphene Oxide Templated Growth and Superior Lithium Storage Performance of Novel Hierarchical $Co_2V_2O_7$ Nanosheets. *ACS Appl. Mater. Interfaces* **2016**, *8*, 2812−2818.
(33) Xiao, M. S.; Yang, D. Z.; Yan, Y. H.; Tian, Y. P.; Zhou, M.; Hao, M. F.; Cheng, R.; Miao, Y. Q. Nanoplates and Nanospheres of $Co_3(VO_4)_2$ as Noble Metal-free Electrocatalysts for Oxygen Evolution. *Electrochim. Acta* **2015**, *180*, 260−267.
(34) Xing, M.; Kong, L. B.; Liu, M. C.; Liu, L. Y.; Kang, L.; Luo, Y. C. Cobalt Vanadate as Highly Active, Stable, Noble Metal-free Oxygen Evolution Electrocatalyst. *J. Mater. Chem. A* **2014**, *2*, 18435−18443.
(35) Liu, M. C.; Kong, L. B.; Kang, L.; Li, X. H.; Walsh, F. C.; Xing, M.; Lu, C.; Ma, X. J.; Luo, Y. C. Synthesis and Characterization of $M_3V_2O_8$ (M = Ni or Co) Based Nanostructures: A New Family of High Performance Pseudocapacitive Materials. *J. Mater. Chem. A* **2014**, *2*, 4919−4926.
(36) Liu, F. M.; Guan, Y. H.; Dai, M. J.; Zhang, H.; Guan, Y. Z.; Sun, R. Z.; Liang, X. S.; Sun, P.; Liu, F. M.; Lu, G. Y. High Performance Mixed-potential Yype NO_2 Sensors Based on Three-dimensional TPB and $Co_3V_2O_8$ Sensing Electrode. *Sens. Actuators, B* **2015**, *216*, 121−127.
(37) Yang, G. Z.; Cui, H.; Yang, G. W.; Wang, C. X. Self-Assembly of $Co_3V_2O_8$ Multilayered Nanosheets: Controllable Synthesis, Excellent Li-Storage Properties, and Investigation of Electrochemical Mechanism. *ACS Nano* **2014**, *8*, 4474−4487.
(38) Abdolmohammad-Zadeh, H.; Rahimpour, E. A Novel Chemosensor For Ag(I) Ion Based on Its Inhibitory Effect on The Luminol-H_2O_2 Chemiluminescence Response Improved by $CoFe_2O_4$ Nanoparticles. *Sens. Actuators, B* **2015**, *209*, 496−504.
(39) Su, L.; Dong, W. P.; Wu, C. K.; Gong, Y. J.; Zhang, Y.; Li, L.; Mao, G. J.; Feng, S. L. The Peroxidase and Oxidase-like Activity of $NiCo_2O_4$ Mesoporous Spheres: Mechanistic Understanding and Colorimetric Biosensing. *Anal. Chim. Acta* **2017**, *951*, 124−132.
(40) André, R.; Natálio, F.; Humanes, M.; Leppin, J.; Heinze, K.; Wever, R.; Schröder, H. C.; Müller, W. E. G.; Tremel, W. V_2O_5 Nanowires with an Intrinsic Peroxidase-Like Activity. *Adv. Funct. Mater.* **2011**, *21*, 501−509.
(41) Zeb, A.; Xie, X.; Yousaf, A. B.; Imran, M.; Wen, T.; Wang, Z.; Guo, H. L.; Jiang, Y. F.; Qazi, I. A.; Xu, A. W. Highly Efficient Fenton and Enzyme-Mimetic Activities of Mixed-Phase VOx Nanoflakes. *ACS Appl. Mater. Interfaces* **2016**, *8*, 30126−30132.
(42) Huang, L.; Niu, Y.; Li, R.; Liu, H.; Wang, Y.; Xu, G.; Li, Y.; Xu, Y. VOx Quantum Dots with Multienzyme-Mimic Activities and the Application in Constructing a Three-Dimensional (3D) Coordinate System for Accurate Discrimination of the Hydrogen Peroxide over a Broad Concentration Range. *Anal. Chem.* **2019**, *91*, 5753−5761.
(43) Yu, Y. Z.; Ju, P.; Zhang, D.; Han, X. X.; Yin, X. F.; Zheng, L.; Sun, C. J. Peroxidase-like Activity of $FeVO_4$ Nanobelts and Its Analytical Application for Optical Detection of Hydrogen Peroxide. *Sens. Actuators, B* **2016**, *233*, 162−172.
(44) Soundharrajan, V.; Sambandam, B.; Song, J.; Kim, S.; Jo, J.; Kim, S.; Lee, S.; Mathew, V.; Kim, J. $Co_3V_2O_8$ Sponge Network Morphology Derived from Metal-Organic Framework as an Excellent Lithium Storage Anode Material. *ACS Appl. Mater. Interfaces* **2016**, *8*, 8546−8553.
(45) Wu, F. F.; Yu, C. H.; Liu, W. X.; Wang, T.; Feng, J. K.; Xiong, S. L. Large-scale Synthesis of $Co_2V_2O_7$ Hexagonal Microplatelets Under Ambient Conditions for Highly Reversible Lithium Storage. *J. Mater. Chem. A* **2015**, *3*, 16728−16736.
(46) Zhao, Y. K.; Liu, Y. D.; Du, X. Q.; Han, R. X.; Ding, Y. Hexagonal Assembly of $Co_3V_2O_8$ Nanoparticles Acting as an Efficient Catalyst for Visible Light-driven Water Oxidation. *J. Mater. Chem. A* **2014**, *2*, 19308−19314.
(47) Qin, W. J.; Su, L.; Yang, C.; Ma, Y. H.; Zhang, H. J.; Chen, X. G. Colorimetric Detection of Sulfite in Foods by a TMB-O_2-Co_3O_4 Nanoparticles Detection System. *J. Agric. Food Chem.* **2014**, *62*, 5827−5834.
(48) Courtney, C. M.; Goodman, S. M.; Nagy, T. A.; Levy, M.; Bhusal, P.; Madinger, N. E.; Detweiler, C. S.; Nagpal, P.; Chatterjee, A. Potentiating Antibiotics in Drug-resistant Clinical Isolates Via Stimuli-activated Superoxide Generation. *Sci. Adv.* **2017**, *3*, e1701776.
(49) Chattopadhyay, K.; Mazumdar, S. Structural and Conformational Stability of Horseradish Peroxidase: Effect of Temperature and pH. *Biochemistry* **2000**, *39*, 263−270.
(50) Ghiyasiyan-Arani, M.; Masjedi-Arani, M.; Salavati-Niasari, M. Size Controllable Synthesis of Cobalt Vanadate Nanostructures with Enhanced Photocatalytic Activity for The Degradation of Organic Dyes. *J. Mol. Catal. A: Chem.* **2016**, *425*, 31−42.
(51) Jia, H. M.; Yang, D. F.; Han, X. N.; Cai, J. J.; Liu, H. Y.; He, W. W. Peroxidase-like Activity of The Co_3O_4 Nanoparticles Used For Biodetection and Evaluation of Antioxidant Behavior. *Nanoscale* **2016**, *8*, 5938−5945.
(52) Liu, Y.; Zheng, Y.; Chen, Z.; Qin, Y. L.; Guo, R. High-Performance Integrated Enzyme Cascade Bioplatform Based on Protein-BiPt Nanochain@Graphene Oxide Hybrid Guided One-Pot Self-Assembly Strategy. *Small* **2019**, *15*, 1804987.
(53) Wang, Y.; Zhang, D.; Wang, J. Metastable Alpha-$AgVO_3$ Microrods as Peroxidase Mimetics for Colorimetric Determination of H_2O_2. *Microchim. Acta* **2018**, *185*, 1−8.
(54) Wu, L. H.; Wan, G. P.; Hu, N.; He, Z. Y.; Shi, S. H.; Suo, Y. R.; Wang, K.; Xu, X. F.; Tang, Y. L.; Wang, G. Z. Synthesis of Porous $CoFe_2O_4$ and Its Application as a Peroxidase Mimetic for Colorimetric Detection of H_2O_2 and Organic Pollutant Degradation. *Nanomaterials* **2018**, *8*, 451−466.
(55) Zhao, T. T.; Jiang, Z. W.; Zhen, S. J.; Huang, C. Z.; Li, Y. F. A Copper(II)/Cobalt(II) Organic Gel with Enhanced Peroxidase-like Activity for Fluorometric Determination of Hydrogen Peroxide and Glucose. *Microchim. Acta* **2019**, *186*, 168.
(56) Zhao, H.; Dong, Y. M.; Jiang, P. P.; Wang, G. L.; Zhang, J. J. Highly Dispersed CeO_2 on TiO_2 Nanotube: A Synergistic Nanocomposite with Superior Peroxidase-Like Activity. *ACS Appl. Mater. Interfaces* **2015**, *7*, 6451−6461.
(57) Zhang, L. L.; Han, L.; Hu, P.; Wang, L.; Dong, S. J. TiO_2 Nanotube Arrays: Intrinsic Peroxidase Mimetics. *Chem. Commun.* **2013**, *49*, 10480−10482.

https://dx.doi.org/10.1021/acsabm.9b01107
ACS Appl. Bio Mater. 2020, 3, 1469−1480

(58) Shi, Y.; Huang, J.; Wang, J. N.; Su, P.; Yang, Y. A Magnetic Nanoscale Fe_3O_4/Pbeta-CD Composite as an Efficient Peroxidase Mimetic for Glucose Detection. *Talanta* **2015**, *143*, 457−463.
(59) Wang, Q. Q.; Zhang, X. P.; Huang, L.; Zhang, Z. Q.; Dong, S. J. One-Pot Synthesis of Fe_3O_4 Nanoparticle Loaded 3D Porous Graphene Nanocomposites with Enhanced Nanozyme Activity for Glucose Detection. *ACS Appl. Mater. Interfaces* **2017**, *9*, 7465−7471.
(60) Weibel, M. K.; Bright, H. J. The Glucose Oxidase Mechanism: Interpretation of the pH Dependence. *J. Biol. Chem.* **1971**, *246*, 2734−2744.
(61) Bright, H. J.; Appleby, M. The pH Dependence of the Individual Steps in the Glucose Oxidase Reaction. *J. Biol. Chem.* **1969**, *244*, 3625−3634.

https://dx.doi.org/10.1021/acsabm.9b01107
ACS Appl. Bio Mater. 2020, 3, 1469−1480